ACS OMEGA

Open Access

http://pubs.acs.org/journal/acsodf

Article

Layer-by-Layer Multitargeting Strategy for Enhanced Photothermal Therapy

Shilei Ren,[#] Qian Wang,[#] Chongqing Zhang,[#] Ruochen Du,[*] Jian Meng,[*] and Ruiping Zhang[*]

Cite This: *ACS Omega* 2025, 10, 5460−5467

Read Online

ACCESS | Metrics & More | Article Recommendations

ABSTRACT: Photothermal therapy (PTT) presents unique advantages, including high temporal and spatial controllability and relatively few toxic side effects. Active targeting modifications of photothermal agents can deliver nanoprobes to tumors more efficiently, reducing toxic side effects while improving efficacy. In this work, the polyphenols, gallic acid, folic acid (FA), hyaluronic acid (HA), and Fe(III) were selected to prepare a self-photothermal nanoplatform Ga/Fe/HA/FA based on polyphenol-metal self-assembly. The self-assembly process synchronously integrated the targeting molecules, folic acid and hyaluronic acid, layer by layer in a polyphenol−metal network, thus realizing the "layer-by-layer targeting" effect. Compared with the traditional targeting modification, the self-assembly multitargeting modification strategy effectively avoided the complicated experimental steps of traditional targeting modification. Meanwhile, it mitigated the off-target risk during blood circulation and improved tumor-targeting efficiency, ultimately augmenting the effectiveness of photothermal therapy.

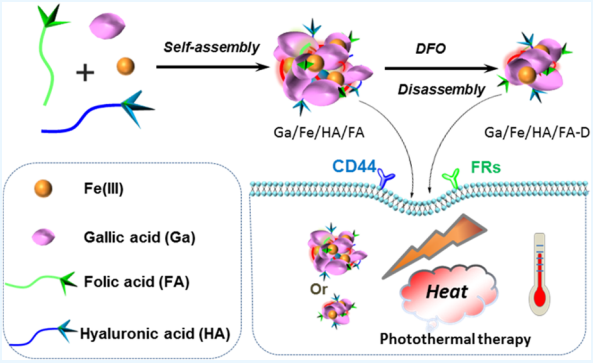

1. INTRODUCTION

Cancer, one of the malignant diseases boasting a high mortality rate, has shown an increasing trend in mortality and morbidity from year to year.[1,2] Surgery, radiotherapy, and chemotherapy are currently the main clinical treatments.[3] The first two treatments suffer from the drawbacks of high trauma and poor healing effects. Chemotherapy is the nonspecific use of chemical drugs to play a therapeutic role, which has the disadvantages of poor specificity, high toxicity and side effects, and easy production of drug resistance.[4] Photothermal therapy (PTT) is an emerging minimally invasive cancer treatment technology developed in recent years. Compared with radiotherapy and chemotherapy, PTT significantly reduces the toxicity to the systemic system.[5,6] With the continuous development of nanotechnology, nanomaterials with photothermal properties have drawn considerable attention from researchers.

Traditional chemotherapeutic drugs enter the human body via oral administration or injection, and after a series of circulation, the amount of drug reaching the tumor tissue site to exert its effect is significantly reduced, resulting in a significant decrease in the bioavailability of the drug, accompanied by a variety of toxic side effects.[7,8] The targeted delivery system obtained by functionalization modification of nanocarriers can accurately deliver drugs to tumor tissues, which can enhance the therapeutic efficacy while reducing toxic side effects simultaneously.[9−11]

Targeted drug delivery is categorized into passive targeting and active targeting. Passive targeting refers to the rapid growth of tumor cells, resulting in excessive secretion of vasopromoting factors in the tumor tissue site, which causes irregularities in the vascular wall of the site and the obstruction of lymphatic return in the tumor tissue site. As a result, the nanodelivery system acts on the tumor tissue through the enhanced permeability and long retention effect.[12] Active targeting refers to the targeting of drug delivery by ligand modification of the nanodrug delivery system to specifically recognize the overexpressed receptors on the surface of tumor cells, such as the CD44 receptor (hyaluronic acid (HA) as the targeting ligand) and folate receptor (folic acid (FA) as the targeting ligand), etc.[13,14]

HA is a natural polysaccharide, and the nanocarriers constructed using HA possess tumor-targeting functions.[15−17] Cheng et al.[18] used bovine serum albumin (BSA) with good biocompatibility to encapsulate contrast agent Gd_2O_3 and sensitizer MoS_2, followed by further targeted modification with HA. Due to the targeting effect mediated by HA and the

Received: August 17, 2024
Revised: November 21, 2024
Accepted: January 27, 2025
Published: February 8, 2025

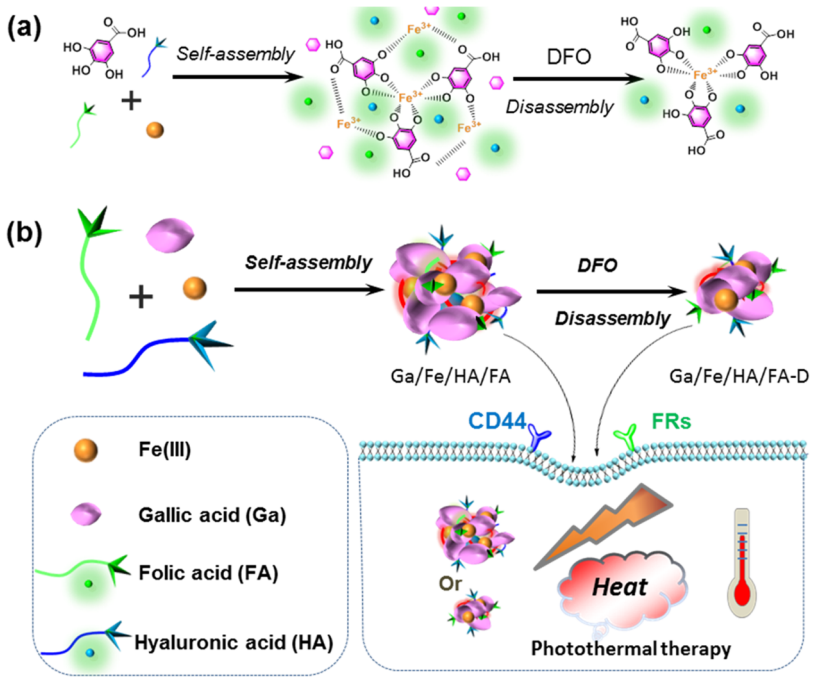

Figure 1. Schematic illustration for the preparation (a) and operation (b) of nanoparticles.

degradability of MoS_2 after reacting with high levels of glutathione in tumor cells, the nanoprobes effectively improve mouse survival rates without significant side effects. Pulakkat et al.[19] used layered techniques to construct HA-modified nanoprobes loaded with the drug doxorubicin (DOX). It was clearly observed through the imaging system that, compared with free DOX, due to the specific targeting of HA to CD44 overexpressed in breast cancer cells, the accumulation concentration of nanoprobes at the tumor site was significantly increased, thus realizing the controlled release of drugs at the tumor site.

Folate receptors FRs are overexpressed in a variety of human cancers, and folate acid is a high-affinity ligand for FRs.[20,21] Nguyen et al.[22] prepared FA-modified targeted probes for the treatment of breast cancer. The probe is surface-modified with FA and internally wrapped with gold nanorods and the drug DOX. The FA-modified probe has a higher cellular uptake rate, indicating its stronger targeting ability and effective inhibition of tumor growth. Tie et al.[23] used FA-modified nanoprobes to deliver the gene BIM-S for the treatment of lung cancer. The translation of the BIM-S gene promotes apoptosis protein BIM, which can specifically inhibit the growth of lung cancer, reduce the number of tumor nodules, and lighten tumor weight.

Recently, the application of HA and FA in a tumor-targeted drug delivery system has received more and more attention from researchers and has become a major research hotspot for tumor-targeted therapy.[24] However, traditional targeted modification involves attaching targeted molecules onto the surface of nanoparticles only through weak interactions such as simple physical adsorption. Due to weak interactions and poor stability, as well as the easy detachment of targeted molecules by nanoparticles during blood circulation. In addition, there are a large number of proteins and enzymes in the blood, which may break down target molecules and cause the probe to lose its targeting effect due to encapsulation. Herein, based on the self-assembly of metal-polyphenols and the strong chelation of iron ions by deferoxamine mesylate (DFO) (Figure 1a), a simple self-assembly strategy assembles layers of folic acid and hyaluronic acid into nanoprobes, and this multitargeted modification method provides a reference for the preparation of efficient diagnostic nanoprobes (Figure 1b). The resulting nanoprobe combines excellent photothermal properties and a good targeting effect.

In clinical cancer treatment, the chemotherapeutic drugs commonly used today not only attack tumor cells but also damage normal cells and cause side effects such as systemic toxicity. They can also induce drug resistance, which reduces the effectiveness of treatment. Meanwhile, the targeting drugs used in the clinic have complicated target modification processes, and most of them are relatively expensive. Boron neutron capture therapy (BNCT) and gadolinium neutron capture therapy (GdNCT) can effectively target tumor tissue and destroy cancer cells. However, there are some controversies and limitations of BNCT and GdNCT, such as the high cost of this treatment modality, limiting their popularity in all medical institutions. Also, there are relatively few indications for BNCT and GdNCT, which are mainly used to treat certain types of cancer such as melanoma and glioma. The nanoprobes Ga/Fe/HA/FA designed in this study based on enhanced permeability retention (EPR) effects[25] can be effectively enriched at the tumor site to achieve a good antitumor effect. In addition, the nanoprobes can be easily modified to provide a layer-by-layer targeting effect, which improves the efficiency of tumor targeting, reduces side effects, and enhances therapeutic efficacy. Moreover, we found that the nanoprobe structure can also be loaded with drugs.[25]

2. EXPERIMENTAL SECTION

2.1. Preparation of Ga/Fe and Ga/Fe/HA/FA. Two milligrams of folic acid was weighed into 2 mL of deionized water and the pH of the solution adjusted to 7 with 0.01 M NaOH. Gallic acid (2.5 mg) was added into 30 mL of deionized water and stirred for 15 min at 1000 rpm, and then

https://doi.org/10.1021/acsomega.4c07611
ACS Omega 2025, 10, 5460−5467

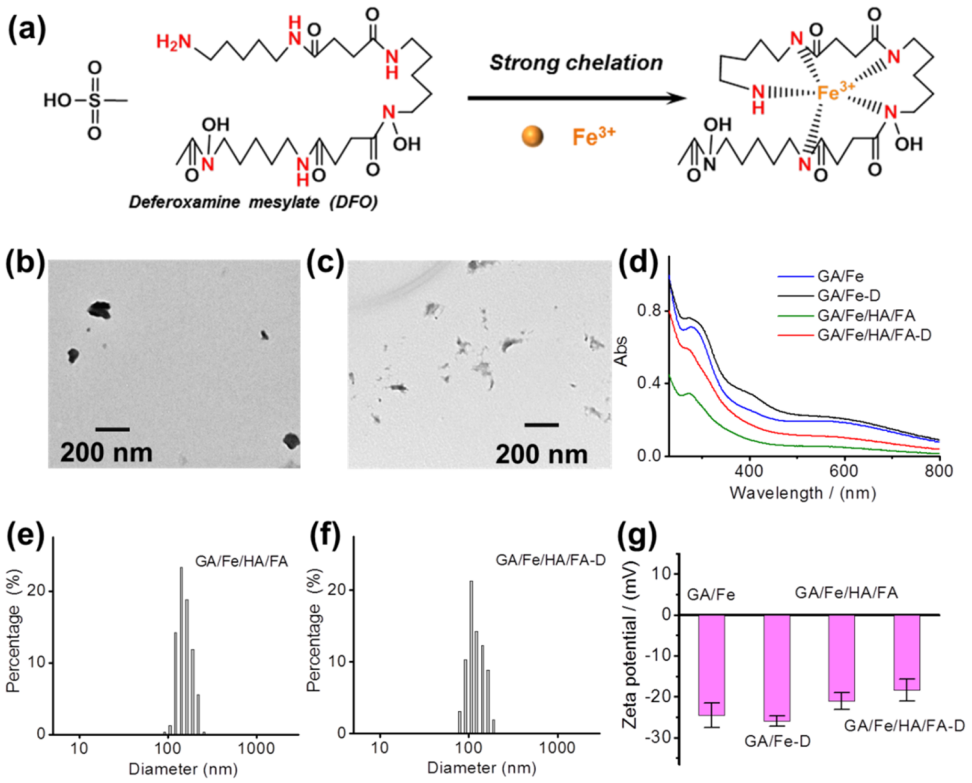

Figure 2. (a) Schematic diagram of the strong chelation of iron ions by DFO. TEM micrograph of (b) Ga/Fe/HA/FA and (c) Ga/Fe/HA/FA-D. (d) UV−vis−NIR absorption spectra of Ga/Fe, Ga/Fe-D, Ga/Fe/HA/FA, and Ga/Fe/HA/FA-D. DLS of (e) Ga/Fe/HA/FA and (f) Ga/Fe/HA/FA-D. (g) ζ potentials of Ga/Fe, Ga/Fe-D, Ga/Fe/HA/FA, and Ga/Fe/HA/FA-D.

the sodium folate solution and 1 mL of hyaluronic acid solution (2 mg/mL) were added and stirred for 15 min. After that, 2 mL of the ferric chloride (200 mM) solution was added to the stirred mixture, and the stirring was stopped after 1 h. Due to self-assembly between polyphenols and metals, as well as hydrogen-bonding electrostatic interactions, gallic acid assembles with trivalent iron ions to form nanoparticles. The resulting mixture was placed in a partitioning chamber. The resulting mixture was dialyzed in a dialysis bag with a molecular weight of 8000−12 000 for 24 h. After dialysis, Ga/Fe/HA/FA was obtained. Meanwhile, the process of preparation without adding folic acid and hyaluronic acid was prepared to obtain Ga/Fe.

2.2. Preparation of Ga/Fe-D and Ga/Fe/HA/FA-D. Five milliliters of each of the Ga/Fe and Ga/Fe/HA/FA solutions was taken. Then, 2 mg/mL DFO was added to the two solutions and stirred for 15 min and the resulting mixtures were placed in a dialysis bag with molecular weights of 8000−12 000 and dialyzed for 24 h. After that, nanoparticles Ga/Fe-D and Ga/Fe/HA/FA-D were obtained.

2.3. Characterization. A JEOL-2100F transmission electron microscope (TEM), Hitachi UH5300 ultraviolet−visible−near-infrared (UV−vis−NIR) spectrometer, Zetasizer Nano ZS90 molecular particle sizing analyzer (dynamic light scattering (DLS)), T460SC thermal imaging camera, and LSR808H near-infrared laser were applied to measure the nanoparticles' properties.

2.4. Photothermal Performance Test. The nanoparticles' solutions were diluted in equal proportions, dispensed into Eppendorf (EP) tubes, and irradiated by an 808 nm laser. Then, the photothermal effect of the probe solutions at different concentrations was recorded by infrared thermography. The solutions were irradiated and cooled every 5 min for three cycles to observe the photothermal stability. An 808 nm laser with a power density of 1 W/cm^2 was used to irradiate 100 μL of the nanoparticles' solution (100 μg/mL) until it was stabilized. Then, the solution was cooled down to room temperature, and the temperature was monitored every 15 s. The temperature was measured with an infrared thermal imaging camera.

2.5. In Vitro Cell Uptake Tests. Different concentrations of nanoparticles were cocultured with 4T1 cells, and the cell activity was detected by the Cell Counting Kit-8 (CCK-8) method. The nanoparticles were mixed with fluorescein isothiocyanate (FITC) in a ratio of 1:8 and stirred in the dark for 1 h. Then, they were repeatedly washed with water using an ultrafiltration centrifuge tube and centrifuged until the centrifugation solution was colorless, resulting in FITC-labeled nanoparticles. The cells were inoculated in 96-well plates with 1×10^4 cells per well and incubated with the Dulbecco's modified Eagle's medium (DMEM) with a 10% fetal bovine serum at 37 °C and 5% CO_2 for 24 h to make the cells adhere to the wall. HA, FA, HA + FA, and phosphate-buffered saline (PBS) were added and cocultivated for 4 h. Then, FITC-labeled nanoparticles were added and cocultivated for 24 h. The medium was removed, and cell nuclei were stained with 4′,6-diamidino-2-phenylindole (DAPI) for 7 min and washed three times with PBS. A fluorescence microscope was used to take pictures to observe the uptake of nanoparticles by the cells.

2.6. Cellular Photothermal Experiments with Nanoparticles. The killing effect of different treatments on tumor cells in vitro was evaluated using a live/dead cell double staining kit (Calcein-AM/propidium iodide (PI)). The 4T1

https://doi.org/10.1021/acsomega.4c07611
ACS Omega 2025, 10, 5460−5467

cells were inoculated into 96-well plates. After their adherent growth, the following groupings were set up: (1) HA group, (2) FA group, (3) HA + FA group, and (4) PBS group. The old medium was discarded and the corresponding nanomedicine was added. The mixture was incubated overnight, irradiated with laser (808 nm) for 7 min, washed three times with PBS, dilute Calcein-AM/PI dye was added, cells were stained for 45 min at 37 °C in a constant temperature shaker, remaining dye was washed off with PBS, the state of the 4T1 cells was observed with an inverted fluorescence microscope, and pictures taken for 1 h. The cells were then incubated for 1 h with a laser (808 nm) for 7 min and washed three times with PBS.

3. RESULTS AND DISCUSSION

Deferoxamine contains a large number of nitrogen atoms, which strongly chelate iron ions (Figure 2a). The resulting nanoprobes were characterized by multiple methods. Transmission electron microscopy revealed that Ga/Fe/HA/FA exhibited a granular morphology (Figure 2b). When nanoparticle Ga/Fe/HA/FA interacted with DFO, DFO strongly chelated the iron ions of Ga/Fe/HA/FA and disintegrated its structure.[25] As seen in Figure 2c, the treated nanoparticles Ga/Fe/HA/FA-D became smaller in size and looser in structure. The nanoparticles were dispersed in water, and their average hydrated particle size was measured by a dynamic light scattering apparatus. Figure 2e,f shows that the hydrated kinetic diameters of Ga/Fe/HA/FA and Ga/Fe/HA/FA-D were 146 and 105 nm, respectively. Meanwhile, four types of nanoparticles had broad absorption from 200 to 800 nm in the UV−vis−NIR region (Figure 2d), and the ζ potential of four types of nanoparticles was negative, with a very small difference in the values (Figure 2g). It was demonstrated that DFO only disintegrated the outer structure of the nanoparticles without breaking their base structure.

The temperature of Ga/Fe and Ga/Fe/HA/FA solutions under different laser power irradiations (Figure 3a,c) was monitored in real time by an infrared thermal imager using 808 nm laser irradiation. The results demonstrated that the nanoprobe solution exhibited laser power-dependent behavior,

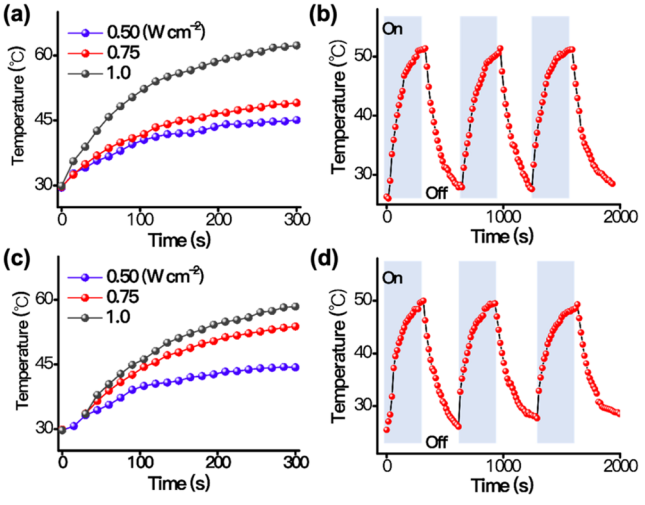

Figure 3. Temperature variations of Ga/Fe (a) and Ga/Fe/HA/FA (c) solution under different laser power irradiations. Temperature changes of Ga/Fe (b) and Ga/Fe/HA/FA (d) solutions over three cycles.

and there was a significant increase in temperature with an increment in laser power. After three rounds of 808 nm laser irradiation, the maximum temperature remained essentially unchanged (Figure 3b,d), indicating the high photothermal stability of Ga/Fe and Ga/Fe/HA/FA.[26]

The temperature of Ga/Fe-D and Ga/Fe/HA/FA-D solutions under different laser power irradiations (Figure 4a,c) was continuously monitored in real time by using an

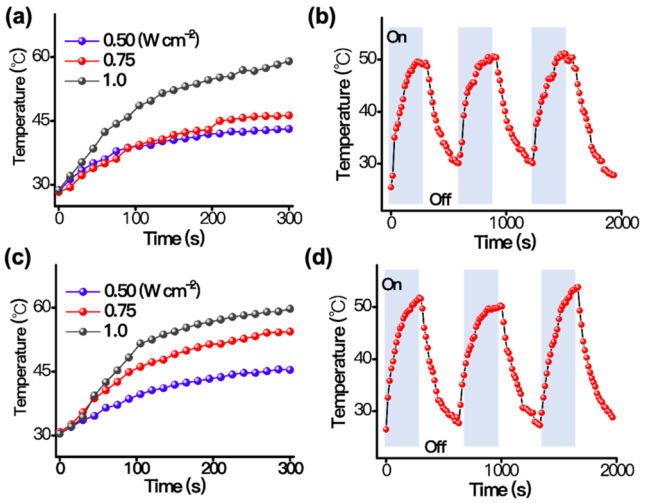

Figure 4. Temperature variations of Ga/Fe-D (a) and Ga/Fe/HA/FA-D (c) solution treated with DFO under different laser power irradiations. Temperature changes of Ga/Fe-D (b) and Ga/Fe/HA/FA-D (d) solutions treated with DFO over three cycles.

infrared thermal imager irradiated by a laser at 808 nm. The results demonstrated that the nanoprobe solution showed a laser power-dependent property, with the temperature increasing significantly with the increase in solution concentration. After three cycles of 808 nm laser irradiation, the maximum temperature remained essentially unchanged (Figure 4b,d), indicating the high photothermal stability of Ga/Fe-D and Ga/Fe/HA/FA-D. Compared to the photothermal properties of Ga/Fe and Ga/Fe/HA/FA nanoparticles, those of the remaining nanoparticles Ga/Fe-D and Ga/Fe/HA/FA-D did not change much after treatment with DFO. This was due to their external structure being only disrupted by DFO.

HA is a natural polysaccharide with good biocompatibility and biodegradability. CD44 is an earlier discovered HA receptor, which facilitates the recognition of nanomaterials modified with HA, and the nanomaterials constructed using HA have tumor-targeting functions.[27] Folate receptor is a common targeting receptor that has been widely studied because it is overexpressed on the surface of various tumor cells. There are four isoforms of FRs, namely, FR-α, FR-β, FR-γ, and FR-δ. Folic acid is a high-affinity ligand for FRs.[28,29]

The cellular uptake assays of nanoparticles were assessed using fluorescence tests to validate their specific targeting properties toward cancer cells. Initially, the cells were coincubated with HA, FA, HA + FA, and blank group (−). Subsequently, the uptake of Ga/Fe and Ga/Fe/HA/FA by 4TI cells was examined to evaluate their targeting ability. As depicted in Figure 5a−e, the cellular uptake rates of Ga/Fe in HA, FA, HA + FA, and blank groups exhibited similarity. Conversely, the uptake rates of Ga/Fe/HA/FA in HA, FA, HA + FA, and blank groups varied greatly, with the highest uptake

https://doi.org/10.1021/acsomega.4c07611
ACS Omega 2025, 10, 5460−5467

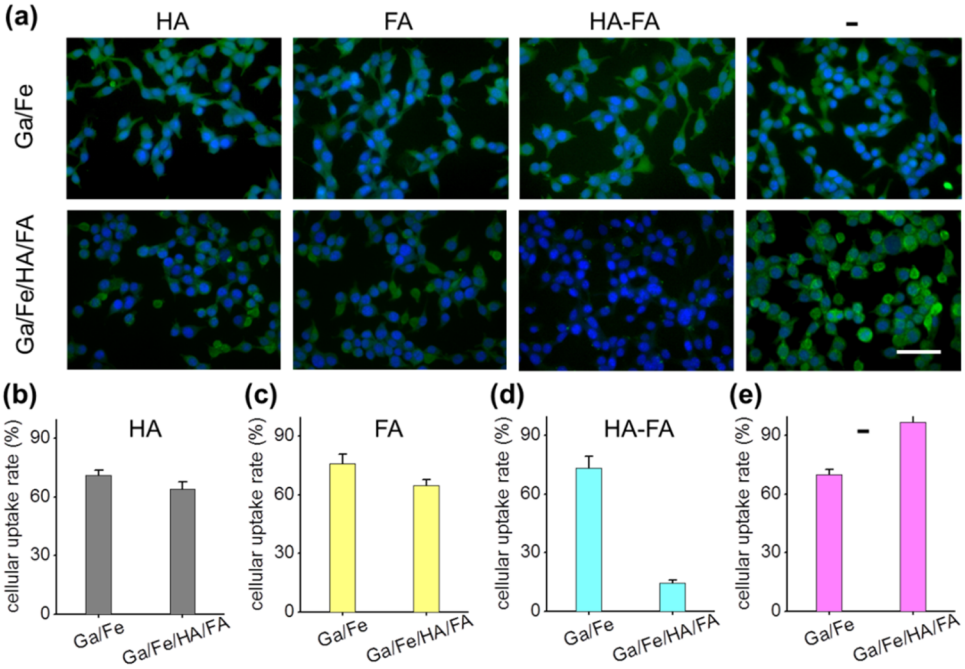

Figure 5. (a) Cellular uptake of nanoparticles Ga/Fe and Ga/Fe/HA/FA. Nanoparticles uptake rate after coincubation of cells with HA (b), FA (c), HA + FA (d), and (−) (e) (scale bar, 250 μm).

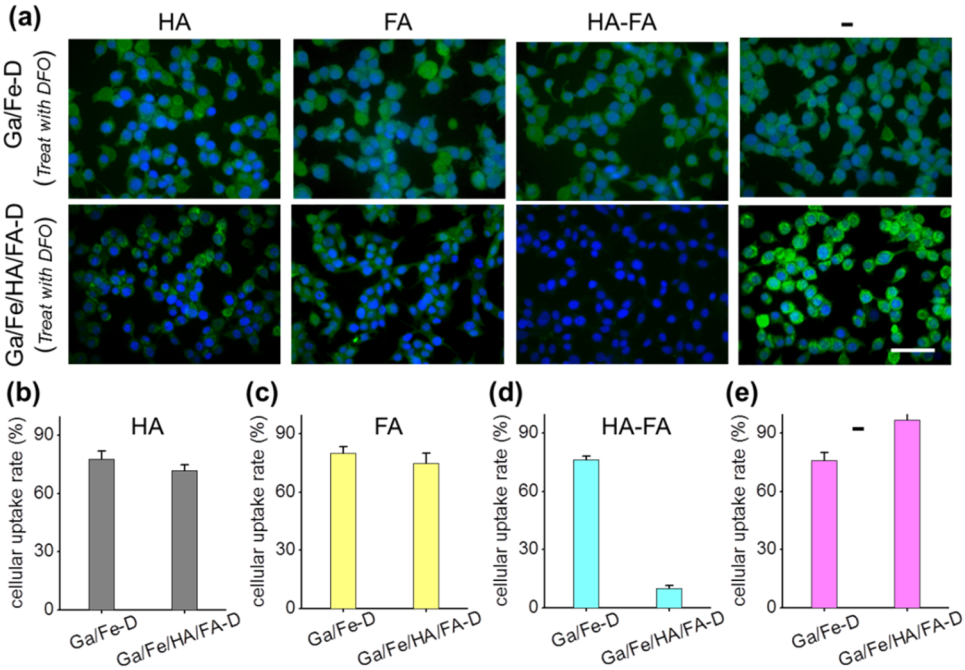

Figure 6. (a) Cellular uptake of nanoparticles Ga/Fe and Ga/Fe/HA/FA. Nanoparticles uptake rate after coincubation of cells with HA (b), FA (c), HA + FA (d), and (−) (e) (scale bar, 250 μm).

rate of 97.0% (Figure 5e) in the blank group and the lowest uptake rate of 14.3% (Figure 5d) in the HA + FA group. This discrepancy can be attributed to the surface of Ga/Fe/HA/FA containing a large number of CD44 and FR receptors. When the cells were coincubated with HA, FA, and HA + FA, HA and FA will occupy the receptors on the surface of the tumor cells, which will not be conducive to their uptake of Ga/Fe/HA/FA. In contrast, a large number of HA and FA receptors on cell surfaces within the blank group effectively recognize bound Ga/Fe/HA/FA nanoparticles, facilitating their internalization into cells via a receptor-mediated endocytosis pathway. These findings indicated that modification with HA and FA enables specific active targeting toward 4T1 cells by Ga/Fe/HA/FA nanoparticles.

To validate the "layer-by-layer targeting" performance of the nanoprobes Ga/Fe/HA/FA, the iron overloading agent DFO was chosen, and DFO strongly chelated the iron ions in Ga/Fe/HA/FA to further disintegrate its structure. It was used to simulate the degradation of the nanoprobes in blood circulation under the action of electrolytes, hormones, and

https://doi.org/10.1021/acsomega.4c07611
ACS Omega 2025, 10, 5460−5467

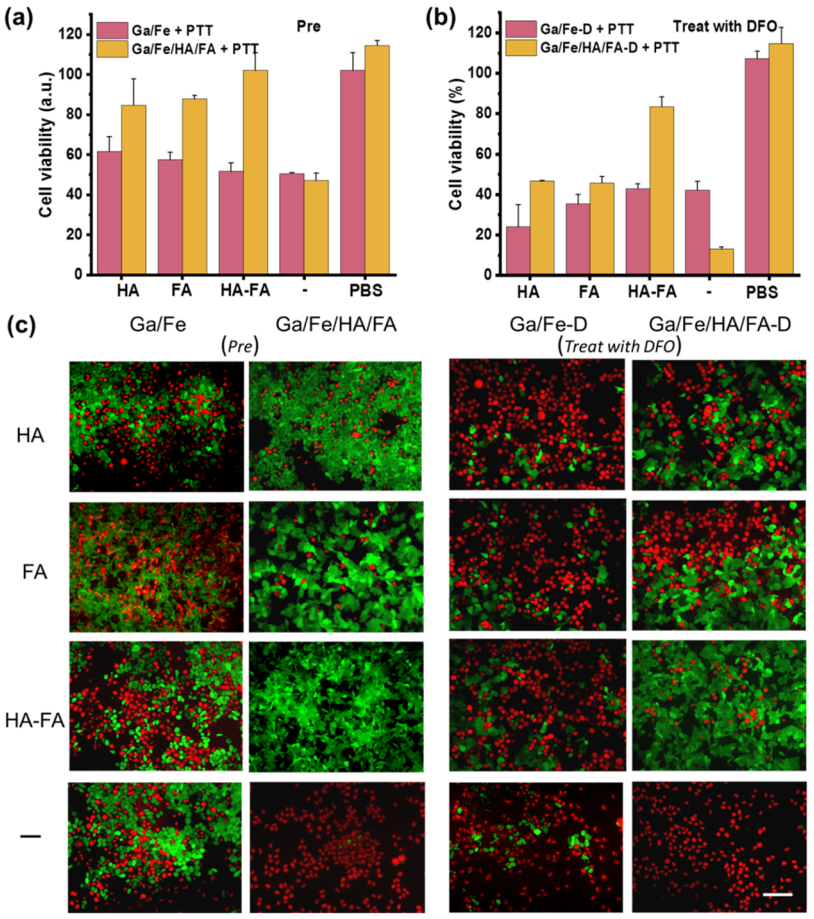

Figure 7. Relative viabilities of 4T1 cells after the incubation with (a) Ga/Fe and Ga/Fe/HA/FA and (b) Ga/Fe-D and Ga/Fe/HA/FA-D. (c) Calcein-AM/PI-stained images for nanoparticles under 808 nm laser irradiation (scale bar, 100 μm).

enzymes. The results of the cell uptake of Ga/Fe and Ga/Fe/HA/FA treated with DFO were similar to those described above. As shown in Figure 6a–e, the cellular uptake rates of Ga/Fe-D in HA, FA, HA + FA, and blank groups were similar. Meanwhile, the uptake rates of Ga/Fe/HA/FA-D in HA, FA, HA + FA, and blank groups varied greatly, with the highest uptake rate of 98.1% (Figure 6e) in the blank group and the lowest uptake rate of 10.0% (Figure 6d) in the HA + FA group. It was further verified that after Ga/Fe/HA/FA treatment with DFO, the remaining nanoparticles Ga/Fe/HA/FA-D still contained a large number of targeting molecules HA and FA. It could still recognize and bind to the receptors CD44 and FRs on the surface of the tumor cells very well and thus specifically and actively target 4T1 cells.

As shown in Figure 7a, the cell survival rates of Ga/Fe + PTT in HA, FA, HA + FA, and blank groups exhibited similar trends. However, the uptake rates of Ga/Fe/HA/FA + PTT in HA, FA, HA + FA, and blank groups varied significantly among these groups, with the highest uptake rate of 102.0% in the blank group and the lowest uptake rate of 47.1% in the HA + FA group. This discrepancy can be attributed to the fact that when the cells were coincubated with HA, FA, and HA + FA, the uptake of the photothermal agent Ga/Fe/HA/FA by the tumor cells was reduced, and the generated photothermal heat became weaker, leading to increased cell survival. The results of cell survival rates of Ga/Fe-D and Ga/Fe/HA/FA-D were similar to those described above. As shown in Figure 7b, the cellular uptake rates of Ga/Fe-D in HA, FA, HA + FA, and blank groups were similar. Meanwhile, the uptake rates of Ga/Fe/HA/FA-D in HA, FA, HA + FA, and blank groups varied greatly, with the highest uptake rate of 83.6% in the blank group and the lowest uptake rate of 13.0% in the HA + FA group.

In addition, fluorescence microscopy was employed to evaluate cellular status using green fluorescence for live cells and red fluorescence for dead cells.[30,31] The majority of cells treated with Ga/Fe + PTT in the HA, FA, or HA + FA group displayed green fluorescence, indicating that their photothermal effect under near-infrared light had minimal damaging effects on cells. In contrast, enhanced red fluorescence was observed for cells treated with Ga/Fe/HA/FA + PTT and Ga/Fe/HA/FA-D + PTT (Figure 7c), indicating reduced ability to damage cells while further confirming improved cellular delivery through targeting strategies. Additionally, all groups showed similar red/green fluorescence after photothermal treatment when using unmodified Ga/Fa nanoparticles. The results of cell live–dead staining after DFO treatment were consistent with the pretreatment trend, further validating that the self-assembly targeting strategy achieves layer-by-layer targeting.

4. CONCLUSIONS

In summary, polyphenol gallic acid, folic acid, hyaluronic acid, and Fe(III) were prepared by one-step self-assembly to obtain the dual-targeting nanoplatform Ga/Fe/HA/FA. Cellular uptake experiments verified that Ga/Fe/HA/FA had a good

https://doi.org/10.1021/acsomega.4c07611
ACS Omega 2025, 10, 5460–5467

targeting effect. Ga/Fe/HA/FA-D was obtained by the partial disintegration of Ga/Fe/HA/FA through treatment with DFO, and cell uptake experiments verified that Ga/Fe/HA/FA-D had a good targeting effect, thus realizing the layer-by-layer targeting effect of nanoplatform. Furthermore, good targeting led to enhanced photothermal therapeutic effects of the nanoparticles.

AUTHOR INFORMATION

Corresponding Authors

Ruochen Du − *Department of Laboratory Animal Center, Shanxi Medical University, Taiyuan, Shanxi 030001, China*; Email: doc_rochandu@sxmu.edu.cn

Jian Meng − *Third Hospital of Shanxi Medical University, Shanxi Bethune Hospital, Shanxi Academy of Medical Sciences, Tongji Shanxi Hospital, Taiyuan 030032, China; The Radiology Department of Shanxi Provincial People's Hospital, Shanxi Medical University, Taiyuan 030001, China*; orcid.org/0009-0009-6920-7994; Email: mengjian@sxmu.edu.cn

Ruiping Zhang − *The Radiology Department of Shanxi Provincial People's Hospital, Shanxi Medical University, Taiyuan 030001, China*; orcid.org/0000-0001-6922-0747; Email: zrp_7142@sxmu.edu.cn

Authors

Shilei Ren − *Third Hospital of Shanxi Medical University, Shanxi Bethune Hospital, Shanxi Academy of Medical Sciences, Tongji Shanxi Hospital, Taiyuan 030032, China; College of Computer Science and Technology, North University of China, Taiyuan 030051, China*

Qian Wang − *The Radiology Department of Shanxi Provincial People's Hospital, Shanxi Medical University, Taiyuan 030001, China*

Chongqing Zhang − *Shanxi Province Cancer Hospital, Shanxi Hospital Affiliated to Cancer Hospital, Chinese Academy of Medical Sciences, Cancer Hospital Affiliated to Shanxi Medical University, Taiyuan 030013, China*

Complete contact information is available at: https://pubs.acs.org/10.1021/acsomega.4c07611

Author Contributions

#S.R., Q.W., C.Z. contributed equally to this work.

Notes

The authors declare no competing financial interest.

ACKNOWLEDGMENTS

This work has been financially supported by the National Key R&D Program of China, 2023YFC3402800, the National Natural Science Foundation of China (Nos. 82120108016 and 82071987), the Key Laboratory of Nanoimaging and Drug-Loaded Preparation of Shanxi Province (No. 202104010910010), and the Natural Science Foundation of Shanxi Province (No. 202403021212272). The authors also acknowledge the Medical Experimental Center of Shanxi Bethune Hospital for providing the necessary equipment for this work.

REFERENCES

(1) Jiang, J. L.; Cui, X. Y.; Huang, Y. X.; Cui, D. X.; et al. Advances and prospects in integrated nano-oncology. *Nano Biomed. Eng.* **2024**, *16*, 152.

(2) Majid, S. K.; Marwa, A. M. H.; Asmaa, H. M. Exploring the role of phytochemicals: effect of [6]-gingerol combined with colloidal gold nanoparticles on thyroid carcinoma cells. *Nano Biomed. Eng.* **2023**, *15*, 36.

(3) Jiang, Y. Y.; Li, J. C.; Zhen, X.; Xie, C.; Pu, K. Y. Dual-peak absorbing semiconducting copolymer nanoparticles for first and second near-infrared window photothermal therapy: a comparative study. *Adv. Mater.* **2018**, *30*, No. 1705980.

(4) Li, J. C.; Xie, C.; Huang, J. G.; Jiang, Y. Y. Semiconducting polymer nanoenzymes with photothermic activity for enhanced cancer therapy. *Angew. Chem., Int. Ed.* **2018**, *57*, 3995.

(5) Liu, C. H.; Chang, Q.; Deng, X. Y.; et al. Rational construction of CQDs-based targeted multifunctional nanoplatform for synergistic chemo-photothermal tumor therapy. *J. Colloid Interface Sci.* **2025**, *677*, 79.

(6) Hu, Z. C.; Zhou, X.; Wang, C. G.; et al. Photothermal amplified multizyme activity for synergistic photothermal-catalytic tumor therapy. *J. Colloid Interface Sci.* **2025**, *679*, 375.

(7) Li, J.; Qiu, L. P.; Xie, S. T.; et al. Engineering a customized nanodrug delivery system at the cellular level for targeted cancer therapy. *Sci. China Chem.* **2018**, *61*, 497.

(8) Li, Y.; Lin, J. Y.; Fan, Z. X.; et al. A small molecule nanodrug consisting of amphiphilic drug-drug conjugate for self-targeted multi-drug delivery and synergistic anticancer effect. *J. Controlled Release* **2017**, *259*, No. e191.

(9) Yan, J. Q.; Long, X. H.; Liang, Y.; et al. Nanodrug delivery systems and cancer stem cells: From delivery carriers to treatment. *Colloids Surf., B* **2022**, *217*, No. 112701.

(10) Qiu, L. P.; Chen, T.; Ocsoy, I.; et al. A cell-targeted, size-photocontrollable, nuclear-uptake nanodrug delivery system for drug-resistant cancer therapy. *Nano Lett.* **2015**, *15*, 457.

(11) Li, Y.; Lin, J. Y.; Cai, Z. X.; et al. Tumor microenvironment-activated self-recognizing nanodrug through directly tailored assembly of small-molecules for targeted synergistic chemotherapy. *J. Controlled Release* **2020**, *321*, 222.

(12) Mahendra, K.; Umesh, K.; Alak, K. S. Therapeutic nanoparticles: recent developments and their targeted delivery applications. *Nano Biomed. Eng.* **2022**, *14*, 38.

(13) Ashique, S.; Sandhu, N. K.; Chawla, V.; Chawla, P. A. Targeted drug delivery: trends and perspectives. *Curr. Drug Delivery* **2021**, *18*, 1435.

(14) Sturari, S.; Andreana, I.; Picollo, F.; et al. Designing functionalized nanodiamonds with hyaluronic acid-phospholipid conjugates for enhanced cancer cell targeting and fluorescence imaging capabilities. *Nanoscale* **2024**, *16*, 11610.

(15) Abatangelo, G.; Vindigni, V.; Avruscio, G.; et al. Hyaluronic acid: redefining its role. *Cells* **2020**, *9*, No. 1743.

(16) Parayath, N. N.; Amiji, M. M. Preparation of Hyaluronic Acid-Based Nanoparticles for Macrophage-Targeted MicroRNA Delivery and Transfection. *Nanoparticles in Biology and Medicine* **2020**, *2118*, 99−110.

(17) Spadea, A.; Rios de la Rosa, J. M.; Tirella, A.; et al. Evaluating the efficiency of hyaluronic acid for tumor targeting via CD44. *Mol. Pharmaceutics* **2019**, *16*, 2481.

(18) Cheng, Y.; Lu, T.; Wang, Y. D.; et al. Glutathione-mediated clearable nanoparticles based on ultrasmall Gd_2O_3 for MSOT/CT/MR imaging guided photothermal/radio combination cancer therapy. *Mol. Pharmaceutics* **2019**, *16*, 3489.

(19) Pulakkat, S.; Balaji, S. A.; Rangarajan, A.; Raichur, A. M. Surface engineered protein nanoparticles with hyaluronic acid based multi-layers for targeted delivery of anticancer agents. *ACS Appl. Mater. Interfaces* **2016**, *8*, 23437.

(20) Josiah, A. J.; Govender, K. K.; Govender, P. P.; Ray, S. S. Advancements and perspectives in folate-based anticancer drugs: bridging quantum and classical mechanics in folate receptor research. *Adv. Theory Simul.* **2024**, *7* (8), No. 2400377, DOI: 10.1002/adts.202400377.

(21) Mashayekhi, F.; Hadipour, E.; Shabani, S.; Salehi, Z. Folate receptor alpha autoantibodies in the serum of patients with relapsing-

remitting multiple sclerosis (RRMS). *Clin. Neurol. Neurosur.* **2024**, *237*, No. 108161.
(22) Nguyen, V. D.; Min, H. K.; Kim, C. S.; et al. Folate receptor-targeted liposomal nanocomplex for effective synergistic photothermal chemotherapy of breast cancer in vivo. *Colloids Surf., B* **2019**, *173*, 539.
(23) Tie, Y.; Zheng, H.; He, Z.; et al. Targeting folate receptor β positive tumor-associated macrophages in lung cancer with a folatemodified liposomal complex. *Signal Transduction Targeted Ther.* **2020**, *5*, No. 6.
(24) Fidan, Y.; Mucaj, S.; Timur, S. S.; Gürsoy, R. N. Recent advances in liposome-based targeted cancer therapy. *J. Liposome Res.* **2024**, *34*, 316.
(25) Meng, J.; Xin, L.; Zou, B. C.; Wang, L.; Zhao, X. H.; Gao, J. F.; Zhang, R. P. A manual controlled theranostic nanoplatform with real-time photoacoustic quantification of drug release for chemo-photothermal therapy. *J. Colloid Interface Sci.* **2023**, *651*, 1020.
(26) Xin, L.; Guo, C. Y.; Gao, J. F.; Zhao, X. H.; Zou, B. C.; Zhang, R. P. A feasible strategy for preparing an all-in-one theranostic nanoplatform. *Mater. Lett.* **2021**, *305*, No. 130825.
(27) Huang, G. L.; Huang, H. L. Hyaluronic acid-based biopharmaceutical delivery and tumor-targeted drug delivery system. *J. Controlled Release* **2018**, *278*, 122.
(28) Assaraf, Y. G.; Leamon, C. P.; Reddy, J. A. The folate receptor as a rational therapeutic target for personalized cancer treatment. *Drug Resistance Updates* **2021**, *7*, 89.
(29) Scaranti, M.; Cojocaru, E.; Banerjee, S.; Banerji, U. Exploiting the folate receptor α in oncology. *Nat. Rev. Clin. Oncol.* **2020**, *17*, 349.
(30) Xin, L.; Gao, J. F.; Zhao, X. H.; Cai, W. W.; Guo, C. Y.; Zhang, R. P. Facile fabrication of biocompatible metal-phenolic based nanoplatform for magnetic resonance-photoacoustic dual-mode imaging. *Mater. Lett.* **2021**, *287*, No. 129259.
(31) Meng, J.; Wang, L.; Zou, B. C.; Ren, S. L.; Zhang, R. P.; et al. Fluorescent-based nanoplatform with real-time quantification of drug release. *ACS Appl. Polym. Mater.* **2023**, *5*, 1539.

https://doi.org/10.1021/acsomega.4c07611
ACS Omega 2025, 10, 5460−5467